

# The mouth of a dense-core vesicle opens and closes in a concerted action regulated by calcium and amphiphysin

Artur Llobet,<sup>1,2</sup> Minnie Wu,<sup>1</sup> and Leon Lagnado<sup>1</sup>

<sup>1</sup>Medical Research Council Laboratory of Molecular Biology, Cambridge CB2 2QH, England, UK

<sup>2</sup>Laboratori de Neurobiologia, Centro de Investigación Biomédica en Red sobre Enfermedades Neurodegenerativas, Institut d'Investigació Biomèdica de Bellvitge, Universitat de Barcelona, L'Hospitalet de Llobregat 08907, Spain

**S**ecretion of hormones and peptides by neuroendocrine cells occurs through fast and slow modes of vesicle fusion but the mechanics of these processes are not understood. We used interference reflection microscopy to monitor deformations of the membrane surface and found that both modes of fusion involve the tightly coupled dilation and constriction of the vesicle. The rate of opening is calcium dependent and occurs rapidly at concentrations  $<5\ \mu\text{M}$ . The fast mode of fusion is blocked selectively by a truncation mutant of amphiphysin.

Vesicles do not collapse when fusion is triggered by strontium, rather they remain locked open and membrane scission is blocked. In contrast, constriction of the vesicle opening continues when endocytosis is blocked by inhibiting the function of dynamin. Thus, fast and slow modes of fusion involve similar membrane deformations and vesicle closure can be uncoupled from membrane scission. Regulation of these processes by calcium and amphiphysin may provide a mechanism for controlling the release of vesicle contents.

## Introduction

The regulated secretion of hormones and neuromodulatory peptides occurs when calcium triggers large vesicles to fuse with the cell surface to release their contents (for review see Rettig and Neher, 2002). After fusion, the membrane must be mechanically deformed to reshape a vesicle and broken to retrieve it from the cell surface. The dynamics of the processes that alter the shape of the vesicle during regulated secretion are not understood, and we have little understanding of their molecular basis.

The first connection between the lumen of the vesicle and the exterior of the cell is termed the fusion pore, which is thought to be similar to an ion channel (Chow et al., 1992; Lindau and Alvarez de Toledo, 2003; Wang et al., 2003). But the fusion pore only allows the vesicle contents to trickle out at a low rate (Gong et al., 2007). Explosive release occurs when the lipid

forming the vesicle merges with the plasma membrane, resulting in an omega-shape profile at the cell surface (Grynszpan-Winograd, 1971; Benedeczy, 1983; Schmidt et al., 1983). After fusion, the opening to the vesicle can close again to allow retrieval of the whole compartment by a process termed “cavitation” (Henkel and Almers, 1996), or the vesicle might collapse into the surface (Patzak and Winkler, 1986). The term “kiss-and-run” has also been used to describe the retrieval of the whole vesicle after fusion, but whereas some workers confine this term to the idea that the release of vesicle contents occurs only through a narrow fusion pore (Gong et al., 2007), others also use it to describe a transient opening formed by merging of the vesicle membrane with the surface (Tsuboi and Rutter, 2003; Fulop and Smith, 2006). The speed of these fusion events is regulated by calcium, with faster events favored at low concentrations generated by low frequency stimulation, and slower fusion and retrieval favored at higher concentrations of calcium generated by stronger stimulation (Fulop et al., 2005; Elhamdani et al., 2006a,b; Fulop and Smith, 2006). It has been proposed

Correspondence to Artur Llobet: allobet@ub.edu; or Leon Lagnado: ll1@mrc-lmb.cam.ac.uk

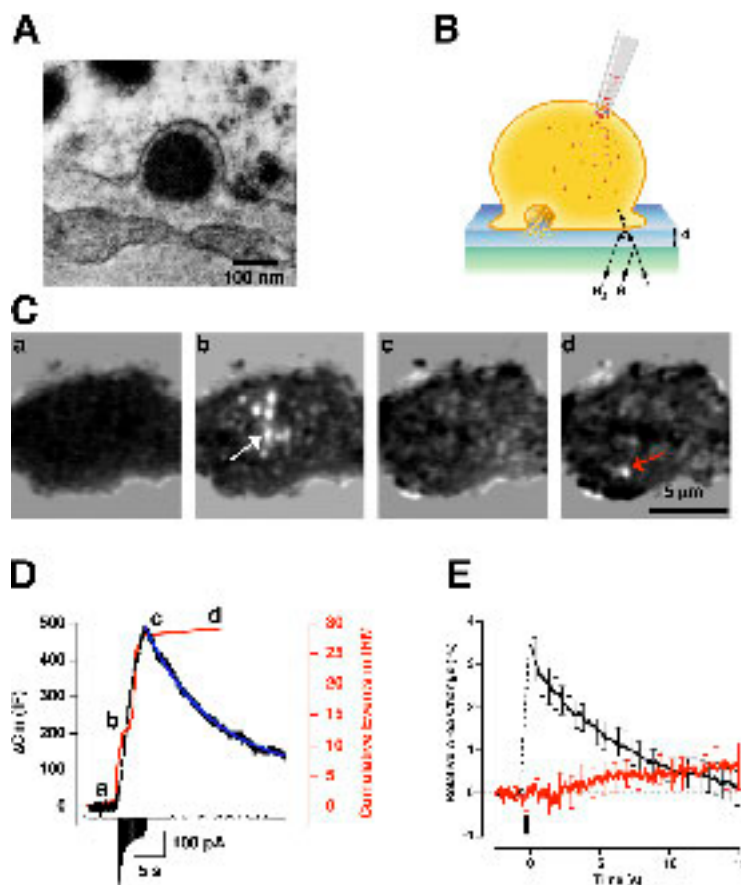
M. Wu's present address is Dept. of Molecular and Cellular Physiology, Stanford University School of Medicine, Stanford, CA 94305.

Abbreviations used in this paper: ANP, atrial natriuretic peptide; BAR, Bin-Amphiphysin-Rv; CCD, charge-coupled device; IRM, interference reflection microscopy; NP, nitrophenyl; ROI, region of interest; TIRF, total internal reflection fluorescence.

The online version of this article contains supplemental material.

© 2008 Llobet et al. This article is distributed under the terms of an Attribution–Noncommercial–Share Alike–No Mirror Sites license for the first six months after the publication date (see <http://www.jcb.org/misc/terms.shtml>). After six months it is available under a Creative Commons License (Attribution–Noncommercial–Share Alike 3.0 Unported license, as described at <http://creativecommons.org/licenses/by-nc-sa/3.0/>).

**Figure 1. Fusion of secretory vesicles visualized by IRM.** (A) An omega shape in a chromaffin cell from hamster adrenal medulla (figure modified from Benedeczy, 1983). (B) Schematic diagram of the experimental configuration showing an omega shape in the footprint. The image obtained by IRM was determined by reflection of light at the interface between the coverslip and medium ( $R_1$ ) and the medium and cell surface ( $R_2$ ). If the distance ( $d$ ) between these two interfaces is of the order of the wavelength of light, then  $R_1$  and  $R_2$  interfere. (C) Difference images from the footprint of a chromaffin cell visualized by IRM. Average of three frames at rest (a), during stimulation (b), immediately after stimulation (c), and 13 s later (d). The stimulus was a train of 24 depolarizing steps 105 ms long, delivered at 5 Hz. (D) The relationship between the cumulative number of events counted in the footprint (red) and the increase in capacitance of the whole cell (black), from the experiment shown in C. Letters a–d show the timing of the corresponding frames in C. The lower trace showing the calcium current also indicates the timing of the stimulus. The blue line describes a single exponential fit ( $\tau = 11.8$  s) to the endocytosis phase. Intensity change as a function of time for the synchronous (white arrow) and asynchronous (red arrow) fusion events indicated in Fig. 1 C. (E) The change in area of the whole cell measured by capacitance (black) compared with the area of the footprint measured by IRM (red). Averaged results from 14 cells. Footprint area did not change significantly when vesicles fused, indicating that they did not collapse.



that slower modes of fusion involve full collapse of the vesicle into the cell surface followed by clathrin-mediated endocytosis, whereas fast events involve kiss-and-run through a fusion pore (Fulop et al., 2005; Elhamdani et al., 2006a,b).

To understand the process of secretion in neuroendocrine cells, we need to investigate the behavior of the omega shape and the molecules that regulate its opening and closing. With this aim, we have used interference reflection microscopy (IRM) to detect the deformations of the surface membrane that occur when vesicles fuse to release hormones and neuromodulatory peptides from adrenal chromaffin cells (for review see Rettig and Neher, 2002). IRM allows membrane deflections of  $<10$  nm to be monitored in real time and reliably signals the fusion of individual dense-core vesicles (Gingell and Todd, 1979; Verschueren, 1985; Llobet et al., 2003; Weber, 2003). We find that fast and slow fusion events triggered at different calcium concentrations all occur by the same fundamental mechanism: the vesicle merges with the surface membrane and the mouth opens and closes in a stereotyped action. Surprisingly, the mouth remained open when secretion was triggered by strontium rather than calcium, demonstrating that vesicles do not normally collapse and that closure is a process distinct from the final step of membrane scission. Introduction of a truncation mutant of amphiphysin blocked fast fusion events and favored slower dilation and constriction of the vesicle. These results indicate that calcium and amphiphysin modulate the release of vesicle contents by controlling the duration of the open omega shape rather than by selecting between kiss-and-run and full-collapse modes of fusion.

## Results

### Evidence that the fusion of vesicles can be visualized by IRM

To investigate the behavior of large dense-core vesicles fusing in chromaffin cells (Fig. 1 A), we monitored the IRM signal generated by deflections of the surface membrane in the region of the cell in close contact with the glass coverslip, the footprint (Gingell and Todd, 1979). When a depolarizing stimulus was applied through a patch pipette, localized bright spots appeared in the footprint, each a fraction of a micrometer in diameter (Fig. 1, B and C). These spots represent a region of the cell surface where destructive interference was lost due to an increase in the distance between the coverslip and surface membrane (Verschueren, 1985). A cumulative plot of IRM events from this footprint is shown by the red trace in Fig. 1 D: they coincided in time with the increase in capacitance of the surface membrane (black trace) and after the peak of the capacitance response there was just one further IRM signal detected in the footprint (Fig. 1 C, c and d). In addition, we have previously found that the capacitance increase per spot is  $\sim 1.4$  fF (Llobet et al., 2003), in close agreement with the mean capacitance of a granule (Ales et al., 1999). We therefore conclude that each bright spot in the IRM image was a direct consequence of the fusion of an individual granule.

In the giant synaptic terminal of retinal bipolar cells, IRM demonstrates that the area of the footprint expands when secretion is stimulated, and there is a precise quantitative and

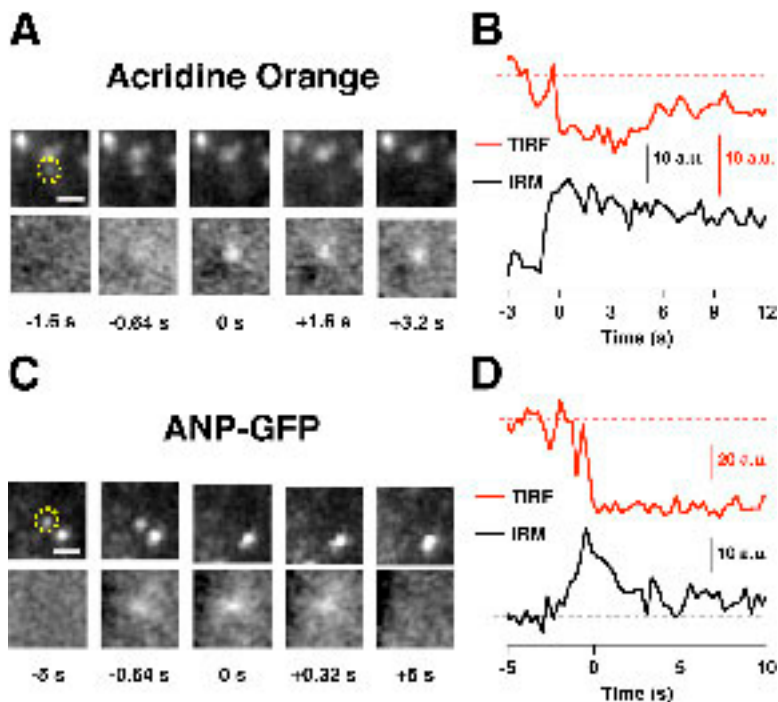


**Figure 2. The release of granule contents coincided with an omega shape visualized by IRM.** (A) The fusion of a vesicle labeled with acridine orange (yellow circle) was visualized by TIRF (top) and IRM (bottom). Images were obtained sequentially at 3 Hz. Disappearance of the granule in the TIRF channel coincided in space and time with a local loss of destructive interference. Bar, 0.5  $\mu$ m. (B) Time course of the change in the intensity of reflected light (black) and fluorescence (red) over an ROI (240  $\times$  240 nm) located in the center of the yellow circle shown in A. Dashed lines indicate the baseline levels of fluorescence (red) and reflected light (black). (C) The fusion of a granule labeled with ANP-GFP (yellow circle) was visualized by sequential TIRF (top) and IRM (bottom). Disappearance of the granule in the TIRF channel coincided in space and time with a local loss of destructive interference. Bar, 0.5  $\mu$ m. (D) Time course of the change in the intensity of reflected light (black) and fluorescence over an ROI located in the center of the yellow circle shown in C. Dashed lines indicate the baseline levels of fluorescence (red) and reflected light (black).

temporal relation with the total surface area of the terminal measured by capacitance (Llobet et al., 2003; Beaumont et al., 2005). In contrast, the stimulation of secretion in chromaffin cells did not cause significant spread of membrane in the region of the footprint. This behavior is shown in Fig. 1 E, which plots the averaged responses of 14 cells to a step depolarization. The stimulus caused a 3.5% increase in the surface area measured by capacitance, but the bounding area of the footprint on the coverslip barely altered. Thus, whereas small synaptic vesicles collapse on fusion, large dense-core vesicles in neuroendocrine cells do not.

Further evidence that IRM signals are generated by vesicle fusion is provided by the observation that they coincide with the release of FM dyes loaded into vesicles and observed by total internal reflection fluorescence (TIRF) microscopy (Llobet et al., 2003). We performed similar tests by observing dense-core vesicles labeled in two other ways: using the recombinant fluorescent probe atrial natriuretic peptide (ANP)-GFP (Johns et al., 2001) or the acidophilic probe acridine orange (Steyer et al., 1997). Both approaches demonstrated that IRM signals observed on depolarization coincided in space and time with the sudden disappearance of labeled granules from the footprint, a hallmark of fusion (Becherer et al., 2007). Fig. 2 shows one of eight events in which granules labeled with acridine orange disappeared on depolarization in precise coincidence with an IRM event (A and B) and one of 16 events in which granules were labeled with ANP-GFP (C and D).

Another approach by which to test the origin of signals generated by IRM is to investigate whether they are altered by experimental maneuvers known to affect granule fusion or retrieval assayed by the capacitance technique or amperometry. Several such tests are provided in subsequent sections. For instance, we demonstrate that the kinetics of the IRM signal are calcium dependent (see Figs. 3–6), and recovery of the signal is

blocked when fusion is triggered by strontium rather than calcium (see Fig. 7). A large number of different experimental observations are therefore consistent with the idea that local and transient invaginations of the surface membrane observed by IRM are omega shapes formed by fused vesicles.

### Analysis of IRM signals

To investigate the information that might be obtained from IRM signals we took a simple measure, the total amount of reflected light from a circular region of interest (ROI) centered on a fusion event. Examples of the way this quantity varies over time are shown in Fig. 3 A for two events, one synchronous with the period of stimulation and another occurring 15 s after calcium channels had closed. Each spot brightens in a small fraction of a second and dims again completely. The theory of image formation by IRM indicates that a gradual brightening could occur if the opening to the granule widens after fusion or if the open granule elongates toward the interior of the cell to increase the path length from the coverslip to the membrane (Gingell and Todd, 1979). The notion that the granule elongates seems very unlikely for three reasons. First, electron microscopy of chromaffin cells has not produced any indication of such behavior (Schmidt et al., 1983). Second, brightening of an IRM spot occurred in a small fraction of a second along a stereotyped time course; if new membrane were being added to the site of fusion, the fusion machinery would have to be very fast and consistent. Third, several groups have shown that the capacitance of an individual vesicle is constant after fusion, indicating that the vesicle cannot elongate by addition of new membrane (Albillos et al., 1997; Ales et al., 1999). The gradual brightening of a spot on granule fusion is also unlikely to reflect dissolution of the proteinaceous core of the granule, at least as its primary cause, because this core is expected to have a refractive index significantly less than the cell membrane (see Materials and methods).

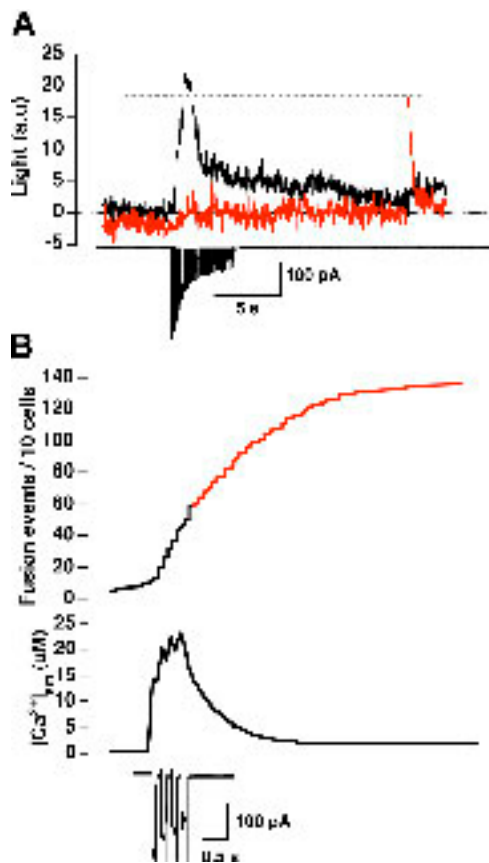


**Figure 3. Synchronous and asynchronous fusion events.** (A) Light intensity change as a function of time for the synchronous and asynchronous fusion events indicated in Fig. 1 C (white and red arrows, respectively). The dotted line indicates the differences in peak amplitudes between the two types of events. (B) Example of the submembranous  $[Ca^{2+}]$  measured in a cell loaded with 0.2 mM Fluo-5N through the patch pipette. Calcium currents were evoked by four 90-ms depolarization steps delivered at 200-ms intervals. The plot below shows the submembranous  $[Ca^{2+}]$  averaged over the whole footprint in a given cell. Similar results were seen for seven other cells. The upper plot shows cumulative exocytosis of synchronous (black) and asynchronous (red) events measured by IRM in response to the same stimulus ( $n = 10$  cells).

In addition, we demonstrate below that the speed with which a spot brightens depends on the cytoplasmic calcium concentration triggering fusion, indicating that this process is regulated by intracellular events. We therefore interpret the rising phase of the IRM signal as representing the dilation of the mouth of the vesicle after it has merged with the cell surface.

Why do spots become dim again? Two mechanisms by which membrane might reattach to the coverslip are collapse and flattening of the fused vesicle or reconstriction of the open mouth. If vesicles collapse, one might expect an expansion of membrane onto the coverslip and an increase in the area of the footprint, as is observed when small synaptic vesicles fuse in retinal bipolar cells (Llobet et al., 2003; Beaumont et al., 2005). Instead, we found that the area of the footprint did not change significantly, even when exocytosis increased the total surface area of the cell by 3–4% (Fig. 1 E). In addition, we demonstrate below that dimming of the IRM signal is dependent on internal calcium, and that membrane invaginations remain locked in the open state when fusion is triggered by strontium. The recovery

in the IRM signal was not, therefore, explicable by passive collapse of the vesicle, and we interpret recovery as constriction of the vesicle mouth.

### Fast and slow modes of vesicle opening and closing

The kinetics of IRM responses depended on the timing of vesicle fusion relative to the opening of calcium channels. For instance, in Fig. 3 A, the event synchronous with the period of depolarization rose more gradually and recovered more slowly than the event occurring after  $Ca^{2+}$  channels had closed (Video 1, available at <http://www.jcb.org/cgi/content/full/jcb.200807034/DC1>). An obvious difference between synchronous and asynchronous release is the  $[Ca^{2+}]$  under the membrane at the time of fusion. To estimate this quantity, we loaded chromaffin cells with 200  $\mu M$  of the calcium indicator Fluo-5N through the patch pipette and imaged the footprint by TIRF microscopy (see Materials and methods). We found that during a depolarizing stimulus, vesicles within  $\sim 150$  nm of the surface membrane were exposed to a  $[Ca^{2+}]$  of at least 20–30  $\mu M$ , but asynchronous release continued after calcium channels closed and the free  $[Ca^{2+}]$  had fallen below 5  $\mu M$  (Fig. 3 B).

To compare the speed of vesicle opening under different conditions, we measured the time for the signal to rise to half maximum ( $D_{1/2}$ ). A histogram of  $D_{1/2}$  for synchronous fusions displayed two peaks and could be described as the sum of two Gaussian distributions with means of 60 and 180 ms (Fig. 4 A, black curve). In contrast, asynchronous events were distributed around a single peak, but again centered on a mean  $D_{1/2}$  of 60 ms (Fig. 4 B, red curve). We could therefore differentiate two populations of vesicle openings, fast and slow. Both occurred while calcium channels were open, but only the fast mode was observed after calcium channels had closed (Fig. 4 C).

The speed of vesicle closing was linked to the rate of opening. Fig. 4 D shows the relation between  $D_{1/2}$  and the time for the IRM signal to recover to half maximum from the peak ( $C_{1/2}$ ). Faster dilation of the vesicle mouth was strongly correlated with faster constriction ( $r = 0.94$ ). Although synchronous events varied widely in the rate of opening and closing, with  $D_{1/2}$  up to 400 ms and  $C_{1/2}$  up to 4 s, asynchronous events were distributed very narrowly, with  $D_{1/2} < 120$  ms and  $C_{1/2} < 2$  s. A value of  $D_{1/2} < 120$  ms and  $C_{1/2} < 2$  s therefore provided two criteria that allowed us to define an event as “fast.” Although all but one of 28 asynchronous fusions were fast, only 130 of 282 synchronous fusions were fast (Fig. 4 C). The peak amplitude of the IRM signal also varied, being lower for fast events compared with slow (Fig. 3 A and Fig. 4 E). This observation suggests that the mouth of the vesicle does not open as widely during fast fusion events.

To visualize the opening and closing of the omega shape more closely, separate movie averages were made of fast and slow events, indexed in time to the frame in which the signal was at its peak (Videos 2 and 3, available at <http://www.jcb.org/cgi/content/full/jcb.200807034/DC1>). A selection of frames from these averages are shown in Fig. 5 (A and B). A notable feature of all fusion events was that, once open, the vesicle did not achieve a stable configuration; the IRM signal began to



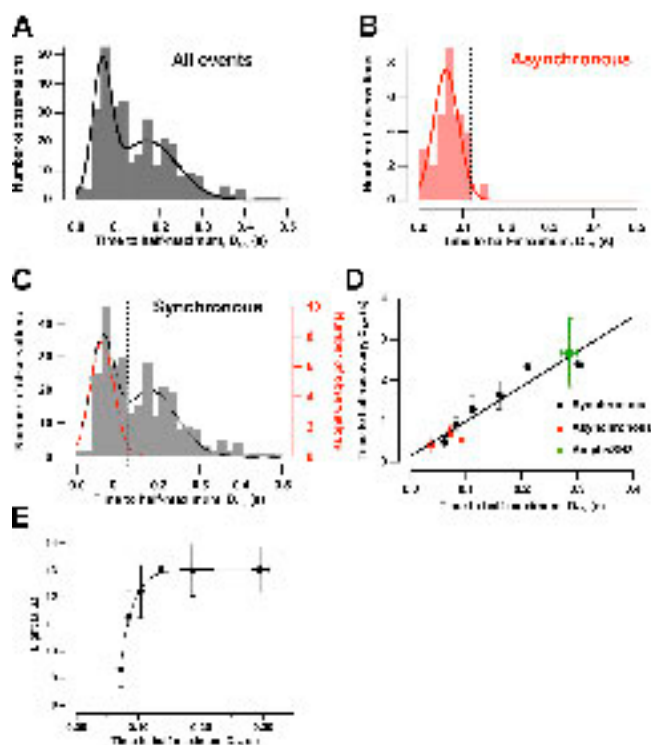


**Figure 4. Fast and slow modes of fusion and retrieval visualized by IRM.** (A) Histogram showing the distribution of  $D_{1/2}$  (time for the IRM signal to increase to half maximum) for 311 fusion events. This population includes both synchronous and asynchronous events. The curve is the sum of two Gaussians, one with a mean of 61 ms and an SD of 41 ms and the second with a mean of 180 ms and an SD of 92 ms. The dashed line shows a value of 120 ms, which was used as a cut-off between fast and slow events. (B) The distribution of  $D_{1/2}$  for 29 asynchronous events described by a single Gaussian with a mean of 61 ms and an SD of 41 ms. The dashed line shows the cut-off value between fast and slow events. (C) The distribution of  $D_{1/2}$  for 282 synchronous events described by the same two Gaussians as in A (black dashed line). 130 of these events were defined as fast and were described by the Gaussian fit used in B (red dashed line). The dashed line shows the cut-off value between fast and slow events. (D) Relation between  $D_{1/2}$  and the time for the IRM signal to recover half maximum from the peak ( $C_{1/2}$ ). Synchronous events in black ( $n = 282$ ) and asynchronous in red ( $n = 29$ ). Line shows a linear fit ( $r = 0.94$ ) through the binned results (solid circles). Events obtained in cells dialyzed with amphiphsin $\Delta$ SH3 are shown in green. Error bars indicate SEM. Note the narrower distribution of asynchronous events. (E) Relationship between the peak amplitude of the IRM signal and  $D_{1/2}$  for synchronous and asynchronous fusions. Bins (average of 18 events) were well described by a single exponential function with a rate constant of  $49.5 \text{ s}^{-1}$  (mean  $\pm$  SEM).

decline immediately after reaching a peak, indicating that the mouth of the vesicle began to close within a fraction of a second (Fig. 5 C). The rising phases of these responses are shown on an expanded time scale in Fig. 5 D, highlighting the explosive opening of the vesicle during fast events. These results demonstrate that fast and slow fusion events both lead to deformations of the surface membrane that can be visualized by IRM.

#### Fast IRM events were triggered at low levels of calcium

Why did vesicles fusing after the closure of calcium channels dilate and constrict more rapidly than those fusing during the depolarizing stimulus? Might vesicles released at low levels of  $\text{Ca}^{2+}$  generate the fastest opening and closing actions? To test

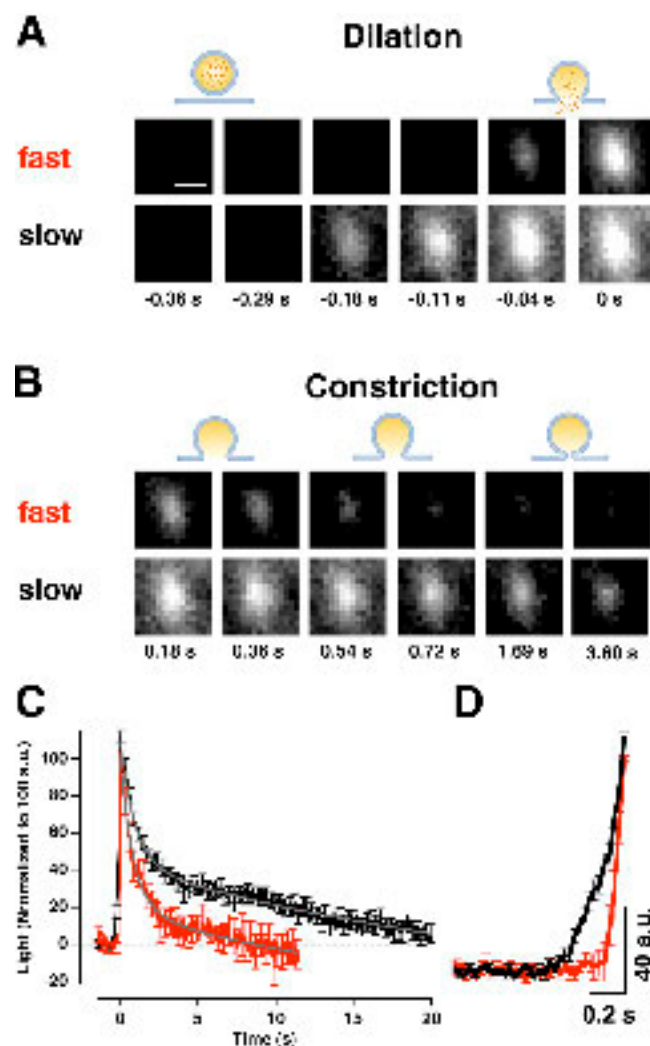
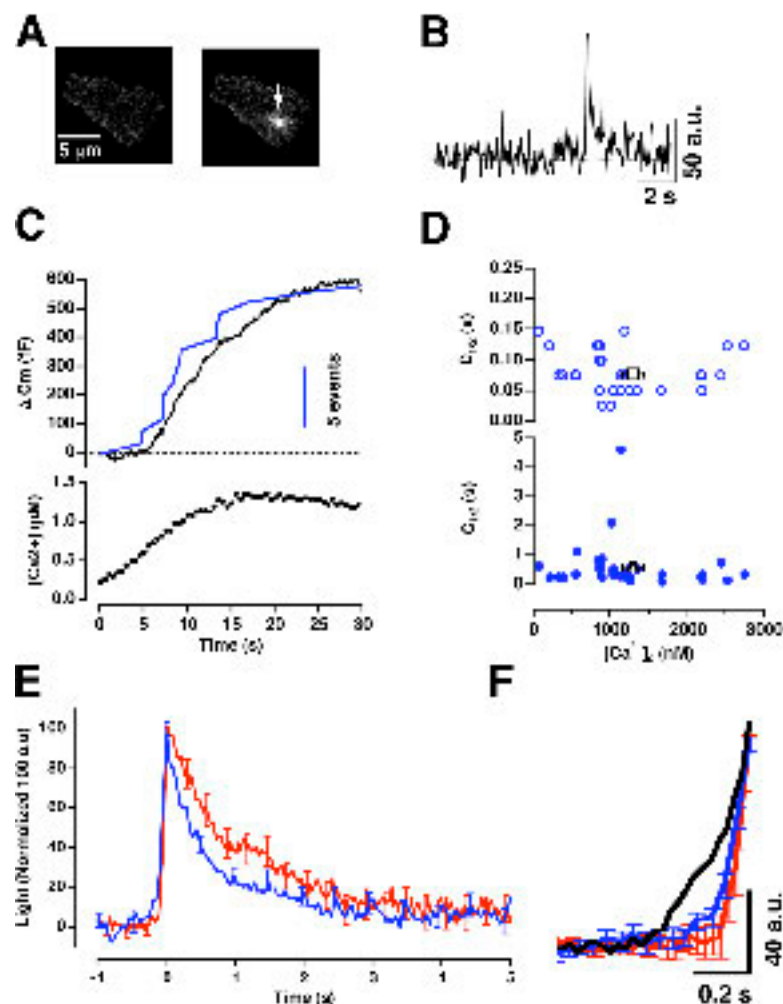


**Figure 5. Dilation and constriction of the mouth of a fused vesicle.** (A) Averaged images from the dilation phase of slow (black;  $n = 6$ ) and fast (red; asynchronous;  $n = 8$ ) fusion events. The peak signal occurred at 0 s. Bar, 0.5  $\mu\text{m}$ . (B) Averaged images from the constriction phase of the same groups of fast and slow fusion events. (C) Time course of the change in the intensity of reflected light averaged from slow (black;  $n = 73$ ) and fast (red;  $n = 16$ ) fusion events. Intensity was averaged over an ROI (252  $\times$  252 nm) centered on the pixel in which the signal was greatest. All the individual events were normalized to a peak value of 100 arbitrary units before averaging. Error bars indicate SEM. (D) Detail of the dilation phase shown in C. Error bars indicate SEM.

this possibility, we used IRM to monitor exocytosis while increasing the free  $[\text{Ca}^{2+}]$  in a chromaffin cell to low micromolar levels by slow photolysis of nitrophenyl (NP)-EGTA, a caged  $\text{Ca}^{2+}$  chelator (Ellis-Davies and Kaplan, 1994). The free  $[\text{Ca}^{2+}]$  was monitored using 0.3  $\mu\text{M}$  Fura-2 ( $K_d = 140 \text{ nM}$ ) or Fura-FF ( $K_d = 5.5 \mu\text{M}$ ). As the  $[\text{Ca}^{2+}]$  was raised, spots appeared in the footprint in parallel with the increase in capacitance of the surface membrane (Fig. 6, A–C). Values of  $D_{1/2}$  and  $C_{1/2}$  did not display any systematic variation with the free  $[\text{Ca}^{2+}]$  when it was below 3  $\mu\text{M}$ ; the mean value of  $D_{1/2}$  was 76 ms and  $C_{1/2}$  was 593 ms (Fig. 6 D). The mean time course of the IRM signal at these concentrations of calcium is shown by the blue trace in Fig. 6 (E and F) and Video 4 (available at <http://www.jcb.org/cgi/content/full/jcb.200807034/DC1>). Dilation and constriction of vesicles

**Figure 6. The mouth of a vesicle opened and closed rapidly at low calcium concentrations.** (A) Difference images from the footprint of a chromaffin cell visualized by IRM. The cytoplasmic  $[Ca^{2+}]$  was gradually raised by slowly uncaging NP-EGTA. Images show the average of three frames at  $\sim 300$  nM  $[Ca^{2+}]$  (left, no activity) and  $\sim 800$  nM  $[Ca^{2+}]$  (right, fusion of a granule arrowed). (B) Time course of the intensity change in an ROI centered on the arrowed region in A. (C) The capacitance increase as a function of time evoked by slowly uncaging NP-EGTA (top, black). A cumulative plot of fusion events visualized by IRM is superimposed in blue. Same cell as in A. The time course of the change in  $[Ca^{2+}]$  is in the bottom panel. (D) Values of  $D_{1/2}$  (open circles) and  $C_{1/2}$  (closed circles) as a function of the  $[Ca^{2+}]$  at which fusion occurred ( $n = 33$ ; 14 cells). Black symbols show mean  $\pm$  SEM. (E) Time course of the change in the intensity of reflected light averaged from fusion events during slow uncaging of NP-EGTA (blue;  $n = 42$ ). For comparison, the red trace shows the average of asynchronous events occurring after a depolarizing stimulus ( $n = 16$ ; Fig. 4). Error bars indicate SEM. (F) Detail of the dilation phases shown in E. For comparison, the black trace shows the average of synchronous events occurring after a depolarizing stimulus ( $n = 73$ ; Fig. 4). Error bars indicate SEM.



fusing at low micromolar levels of  $Ca^{2+}$  was very similar to those fusing asynchronously after a depolarizing stimulus (Fig. 6, E and F, red traces).

Recent experiments using amperometry and the capacitance technique have also demonstrated that a fast mode of fusion predominates at low micromolar levels of calcium (Fulop et al., 2005; Elhamdani et al., 2006a,b; Fulop and Smith, 2006). These authors have termed fast events kiss-and-run, but we do not believe that they can occur through a fusion pore just 1–2 nm in diameter, as this would not generate an IRM signal. It seems that most of the fusion events termed kiss-and-run are actually a fast form of cavicapture.

#### Calcium-dependent constriction of the vesicle mouth

Why are vesicles fusing at high levels of calcium retrieved more slowly? One suggestion is that they collapse and flatten into the surface membrane, requiring the invagination of a new vesicle (Fulop et al., 2005; Elhamdani et al., 2006a,b; Fulop and Smith, 2006). We found, however, that fast and slow events detected by IRM were qualitatively similar, both involving the retrieval of the intact vesicle (Fig. 5 and Videos 2 and 3). This interpretation was strongly supported by the observation that the IRM signal did not recover when fusion was triggered by the influx of stron-

tium instead of calcium (Fig. 7 A); all vesicles remained locked in the open state, irrespective of whether they fused synchronously or asynchronously. The mean of these IRM responses is shown in Fig. 7 (B and C). The closure of the vesicle mouth was dependent on calcium, and strontium could not substitute. These results provide further evidence that the decline in the IRM signal is a regulated process and that the omega shape formed on fusion does not collapse passively. Taraska et al. (2003) used TIRF microscopy to investigate the behavior of individual vesicles after fusion and also concluded that many maintain their identity before resealing to be retrieved intact.

#### Constriction of the vesicle mouth could be uncoupled from membrane scission

What are the molecular processes that alter the shape of the membrane as the omega shape opens and closes? Several proteins have been shown to interact with membrane lipids to deform the bilayer, most notably dynamins (Praefcke and McMahon, 2004), and proteins containing epsin N-terminal homology domains, such as epsin (Hurley and Wendland, 2002), or Bin-Amphiphysin-Rv (BAR) domains, such as amphiphysin (Lee and Schekman, 2004; Peter et al., 2004). Many of these bind preferentially to membranes with a certain degree of curvature (Itoh and De Camilli, 2006), leading to the suggestion that they

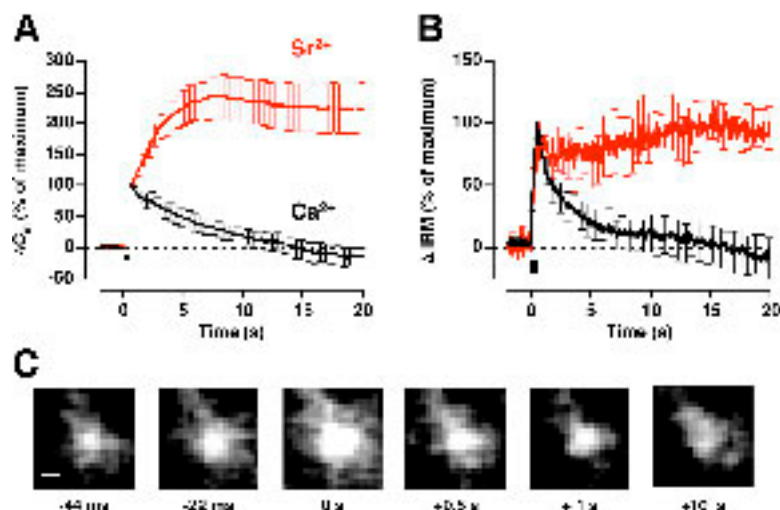


**Figure 7. Closure of the vesicle mouth and membrane retrieval were blocked by  $\text{Sr}^{2+}$ .** (A) The change in capacitance in response to stimulation in the presence of 2.5 mM  $\text{Ca}^{2+}$  (black; 9 cells) or 10 mM  $\text{Sr}^{2+}$  (red; 11 cells). Error bars indicate SEM. Strontium triggered fusion and a large amount of asynchronous release, but there was no net retrieval of membrane, indicating that endocytosis was inhibited. Dashed line indicates the baseline capacitance. (B) Comparison of the IIR response in  $\text{Ca}^{2+}$  (black) and  $\text{Sr}^{2+}$  (red). The response in  $\text{Sr}^{2+}$  is averaged from 9 synchronous and 11 asynchronous events because the two populations could not be distinguished. Error bars indicate SEM. (C) Average images of a single granule fusion in 10 mM  $\text{Sr}^{2+}$  ( $n = 6$ ). Bar, 0.5  $\mu\text{m}$ .

will be recruited sequentially at the appropriate time and place to drive endocytosis forward (Lee and Schekman, 2004; McMahon and Gallop, 2005). In this scenario, the last protein to be recruited is dynamin, a GTPase which constricts and breaks membrane in a wide variety of cells. Fast and slow modes of endocytosis in chromaffin cells are both dependent on the action of dynamin (Artalejo et al., 2002), and one of the key proteins recruiting dynamin to a vesicle is amphiphysin (Wigge et al., 1997). We therefore investigated the roles of dynamin and amphiphysin during the opening and closing of the vesicle mouth.

To assess the timing of dynamin action, we monitored membrane scission using the capacitance technique while also measuring the IIR signal. Fig. 8 A shows the synchronous signals averaged from 42 events in nine cells stimulated for 0.5 s. The initial rate of fall in membrane area over the first second after the stimulus was  $19 \pm 0.7\% \text{ s}^{-1}$  (mean  $\pm$  SD), whereas the IIR signal originating from fused vesicles declined at a rate of  $45 \pm 2\% \text{ s}^{-1}$ . These measurements were repeated after inhibiting the function of dynamin using two different approaches. The first was to introduce the SH3 domain of amphiphysin into chromaffin cells through a whole cell pipette containing 480  $\mu\text{M}$ . The SH3 domain of amphiphysin binds to the proline-rich domain of dynamin to prevent its recruitment to the plasma membrane (Wigge et al., 1997; Holroyd et al., 2002), an action that can be mimicked by the SH3 domains of other proteins. The second approach for inhibiting the action of dynamin was to substitute GTP inside the cell with GTP- $\gamma$ -S to block GTP hydrolysis, a maneuver that allows dynamin recruitment but blocks membrane scission (Takei et al., 1995). In both cases, endocytosis from the cell surface was barely apparent, whereas the IIR signal decayed to baseline with a time course that did not differ significantly from controls, as assessed with an ordinary analysis of variance test (Fig. 8, B and C). Therefore, membrane scission by dynamin did not play an essential role in closing the omega shape.

The faster fall in the IIR signal compared with the capacitance signal might be expected if constriction of the vesicle mouth precedes its removal from the cell surface (Fig. 8 A). Similarly, closure of the omega shape even when membrane scission is blocked (Fig. 8, B and C) would be consistent with a model in

which dynamin is only recruited to the neck of the vesicle after it has become very narrow and local membrane curvature is high (Holroyd et al., 2002; Lee and Schekman, 2004; Tsuboi et al., 2004). A key prediction of this model is that preventing constriction of the vesicle will prevent the recruitment of dynamin and, therefore, block membrane scission. Figs. 7 and 8 show that this is indeed the case. Stimulation of exocytosis in strontium blocked recovery of the IIR signal and also blocked membrane retrieval assayed by the capacitance technique (Fig. 7 A; Artalejo et al., 2002). A second maneuver that blocked both endocytosis and

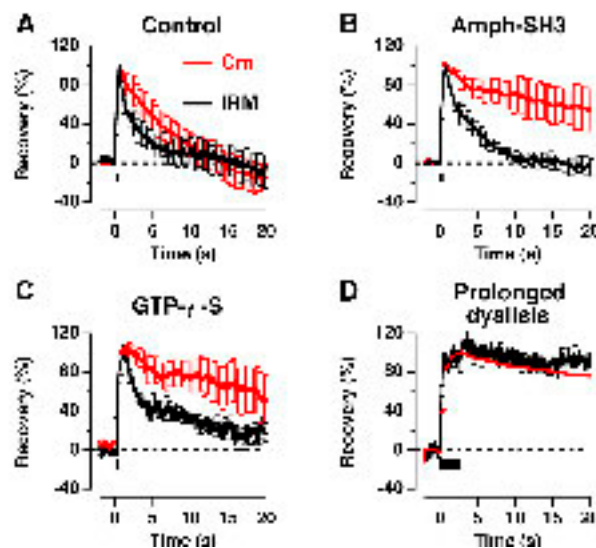


**Figure 8. Closure of the mouth to a fused vesicle was dependent on dialysis time and independent of dynamin activity.** (A) Comparison of the change in capacitance (red) and the IIR signal (black) triggered by a depolarization lasting 0.5 s. Simultaneous measurements were made in nine cells, and only synchronous IIR signals were averaged. Both measurements are normalized. In A–D, the dashed line indicates the baseline levels of capacitance and reflected light and error bars indicate SEM. (B) Intracellular dialysis with 480  $\mu\text{M}$  of amphiphysin-SH3 domain blocked endocytosis assayed by capacitance (red;  $n = 5$ ), but the IIR signal recovered normally (black;  $n = 7$ ). (C) Intracellular dialysis with 1 mM GTP- $\gamma$ -S blocked endocytosis assayed by capacitance (red;  $n = 11$ ). The IIR signal recovered to baseline, although more slowly than controls in A. (D) Simultaneous capacitance and IIR recording in a cell dialyzed for 18 min. The stimulus was a train of 5  $\times$  200-ms depolarizations.



recovery of the IRM signal was prolonged dialysis of the cell through the patch pipette (Fig. 8 D). The inhibition of endocytosis by dialysis has been attributed to the loss of diffusible cytoplasmic factors (Smith and Neher, 1997), and it seems that constriction of the vesicle is also dependent on these.

### An amphiphysin truncation mutant blocked fast fusion events

Amphiphysin is the archetypal member of a family of proteins that can generate membrane curvature through a BAR domain preceeded by an amphipathic helix at the N terminus (Lee and Schekman, 2004; Peter et al., 2004). Amphiphysin plays a key role in clathrin-mediated endocytosis, and like other proteins containing N-BAR domains, it can directly tubulate liposomes without the addition of dynamin or GTP (Takei et al., 1999). Intriguingly, the GTPase activity of dynamin associated with amphiphysin varies according to the curvature of the membrane to which amphiphysin is bound (Yoshida et al., 2004). Curvature is expected to be highest at the neck of a vesicle, leading to the suggestion that amphiphysin might act as a sensor of curvature to regulate membrane scission (Peter et al., 2004). The SH3 domain of amphiphysin also binds the proline-rich domain of synaptojanin 1, a polyphosphoinositide phosphatase that is also thought to have a role in clathrin-mediated endocytosis (Gad et al., 2000).

To investigate how amphiphysin might be involved in the processes of cavicapture, we used a truncation mutant lacking the SH3 domain, thereby preventing recruitment of dynamin and synaptojanin. This amphiphysin $\Delta$ SH3 mutant retains the N-BAR domain and clathrin and adaptor binding motifs, so it is expected to interact with membrane and other binding partners. Amphiphysin $\Delta$ SH3 was introduced into chromaffin cells through a whole-cell pipette containing 20  $\mu$ M and the IRM responses measured during and after depolarization. The mean time for vesicle opening ( $D_{1/2}$ ) for synchronous events in the presence of amphiphysin $\Delta$ SH3 was  $290 \pm 16$  ms, which is significantly longer than those triggered by depolarization under normal conditions or by release of caged calcium (Fig. 9, A and B; and Fig. 4 D). Fig. 9 C shows the distribution of  $D_{1/2}$  values for synchronous fusion events in the presence of amphiphysin $\Delta$ SH3; all openings occurred in 120 ms or more so none could be classified as fast. Further, asynchronous events, which are normally all fast (Fig. 4 B), became significantly prolonged on average (Fig. 9 D). Amphiphysin $\Delta$ SH3 therefore inhibited fast events to favor slower opening and closing of the vesicle. Treatment with amphiphysin-SH3 or GTP- $\gamma$ -S did not significantly alter the speed of opening.

How did the slower closure of vesicles in the presence of amphiphysin $\Delta$ SH3 affect their rate of retrieval? To answer this question, we monitored endocytosis using the capacitance technique (Fig. 9 E). In control conditions, endocytosis proceeded with a rate constant of  $0.12 \pm 0.07$  s $^{-1}$  ( $n = 13$ ), whereas in the presence of amphiphysin $\Delta$ SH3 the rate constant was  $0.06 \pm 0.05$  s $^{-1}$  ( $n = 9$ ). Calcium currents were comparable in both conditions (Fig. 9 F). The longer-lived omega shape in the presence of amphiphysin $\Delta$ SH3 (Fig. 9, A–D) was therefore correlated with a slowing of the mean rate of endocytosis, providing further evidence that closure of the vesicle mouth preceded membrane scission by dynamin.

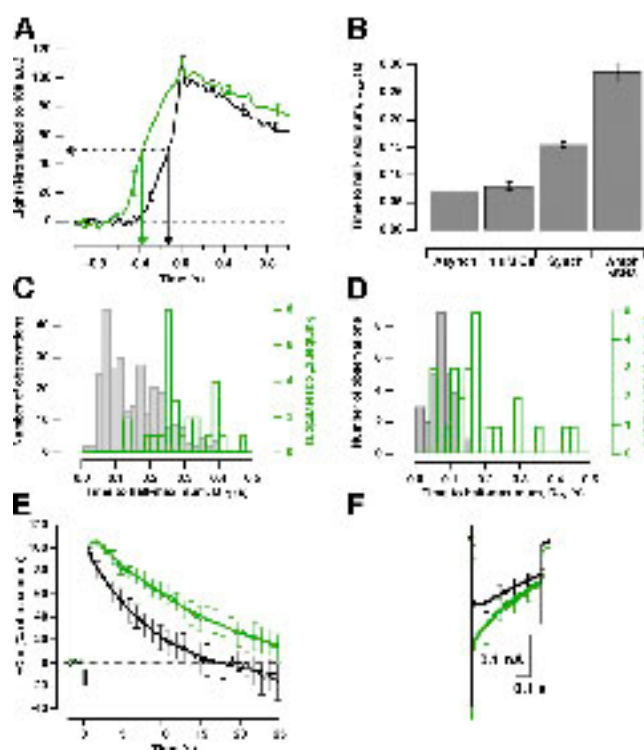


**Figure 9. Effect of amphiphysin truncation mutant on fusion events visualized by IRM.** (A) Time course of the IRM signal averaged from synchronous fusion events in control conditions (black) and in cells dialyzed with a pipette solution containing 20  $\mu$ M of amphiphysin $\Delta$ SH3 (green). The arrows indicate the time to half maximum ( $D_{1/2}$ ). Dashed line indicates the baseline level of reflected light. Error bars indicate SEM. (B) Mean values of  $D_{1/2}$  for fusion events observed asynchronously, after uncaging calcium to levels of  $\sim 1$   $\mu$ M, synchronously under control conditions, and synchronously in the presence of 20  $\mu$ M of amphiphysin $\Delta$ SH3. Error bars indicate SEM. (C) Distribution of time to  $D_{1/2}$  values for synchronous events under control conditions (gray) and after the introduction of amphiphysin $\Delta$ SH3 (green). (D) Distributions for asynchronous events (gray) and during dialysis with 20  $\mu$ M of amphiphysin N-BAR domain (green). (E) Mean change in capacitance in response to a 0.5-s stimulation in control conditions (black; 13 cells) and in cells dialyzed with 20  $\mu$ M of amphiphysin $\Delta$ SH3 (green; 9 cells). Dashed line indicates the baseline level of capacitance. Error bars indicate SEM. (F) The presence of 20  $\mu$ M of amphiphysin $\Delta$ SH3 did not modify calcium currents. Error bars indicate SEM.

## Discussion

### Fast and slow vesicle fusion visualized by IRM

The mechanical behavior of a secretory vesicle has long been the subject of debate, and the molecules that regulate deformation of the membrane have not been identified. Using IRM, we have visualized omega shapes formed at the membrane surface and find that the mouth of a large vesicle opens and closes in a concerted action, the speed of which is regulated by calcium and amphiphysin.

The secretory process had the following basic features: (a) the opening of the omega shape dilated to a maximum within hundreds of milliseconds, (b) the opening was not stable, but began to constrict immediately, (c) the rate of constriction was correlated with the rate of dilation, (d) constriction did not occur when fusion was triggered by strontium, (e) vesicles fusing at low levels of calcium dilated more rapidly than those fusing



at high calcium, (f) neither dilation nor constriction were affected by blocking endocytosis at a step requiring the action of dynamin, and (g) antagonizing the action of amphiphysin selectively blocked fast events.

Evidence that a secretory vesicle can be retrieved intact after fusion has also been obtained using the capacitance technique (Neher and Marty, 1982), by TIRF microscopy (Taraska et al., 2003; Perrais et al., 2004; Taraska and Almers, 2004), and by imaging of plasma membrane lawns (Holroyd et al., 2002). The evidence of Taraska et al. (2003) is particularly direct. Using TIRF microscopy, they imaged a fluorescent marker in the cytosol and found that vesicle fusion created a shadow where the vesicle excluded the marker from the evanescent field. These shadows were long lived, indicating that granules did not collapse; the recapture of a vesicle in this state has been termed cavicapture (Perrais et al., 2004) and we believe that this is the best term to describe the events observed by IRM. The fact that IRM detects fast and slow modes of secretion triggered at different levels of calcium indicates that cavicapture can be regulated by calcium and occurs in seconds (Figs. 3–6 and Videos 2 and 3). Others have suggested that the faster mode of fusion occurring at lower levels of calcium reflects kiss-and-run through a fusion pore (Fulop et al., 2005; Elhamdani et al., 2006a), but our results demonstrate that kiss-and-run is certainly not the exclusive mode of secretion under these conditions.

#### Modulation of dilation and constriction by calcium

IRM measurements demonstrate that calcium regulates both the opening and closing of the vesicle mouth, with vesicles primed to be released at low micromolar levels of  $\text{Ca}^{2+}$  expanding fastest (Figs. 3–7). These results immediately suggest the possibility of a link between the dilation of the open mouth of the vesicle and the  $\text{Ca}^{2+}$ -sensitive step triggering fusion or even the preceeding priming process that is also  $\text{Ca}^{2+}$  sensitive (for review see Rettig and Neher, 2002). The  $\text{Ca}^{2+}$  sensor controlling regulated secretion is synaptotagmin, which has multiple isoforms and binds divalents through C2 domains (Sudhof, 2002). In PC12 cells, the transition from a narrow fusion pore to a wider connection is more likely to occur in vesicles containing synaptotagmin I compared with those expressing synaptotagmin IV (Wang et al., 2001), which correlates with synaptotagmin I having the higher affinity for  $\text{Ca}^{2+}$ .

Two observations indicate that calcium also regulates resealing of the vesicle mouth. The IRM signal generated by vesicles fusing asynchronously or at low levels of calcium declined more rapidly than synchronous events (Fig. 4 D and Fig. 6), and vesicle closure was blocked when fusion was triggered by strontium instead of calcium (Fig. 7 A). These differences in the kinetics of closure may also reflect the properties of different synaptotagmin isoforms, which have variable affinities for strontium compared with calcium (Bhalla et al., 2005). But there is a second qualitative difference in the effects of the two divalents on synaptotagmin: whereas calcium induces binding of the C2 domains to SNARE proteins, strontium does not (Shin et al., 2003). Might the binding of synaptotagmin to SNAREs cause the closure of the vesicle mouth?

How do variations in the kinetics of vesicle opening and closing affect release of vesicle contents? Amperometry demonstrates that catecholamine release occurs in a fraction of a second after the vesicle membrane merges with the cell surface (Ales et al., 1999), so we expect that both fast and slow fusion events will effectively release water-soluble catecholamines. But chromaffin cells also release several peptides and hormones, and TIRF microscopy demonstrates that these are released on a time scale of seconds with molecules of different sizes released at different rates (Barg et al., 2002; Taraska et al., 2003). Fulop et al. (2005) have recently demonstrated that differential transmitter release is of physiological significance, being regulated by the electrical activity of the chromaffin cell; under basal firing conditions, catecholamines are released, whereas at higher firing rates neuropeptides are also secreted.

#### Toward a molecular understanding of dilation and constriction

What are the molecular processes that deform the membrane as the omega shape opens and shuts? In this study, we have investigated the roles of two proteins which have a key role in endocytosis, dynamin and amphiphysin. We find that membrane scission by dynamin is not involved in constricting the mouth of the open vesicle (Fig. 8). Further, membrane retrieval was blocked under conditions in which the vesicle failed to close (Figs. 7 and 9), suggesting that this last step in endocytosis did not begin until the mouth of the vesicle had become very narrow. These results are also consistent with the observation that dynamin is recruited to the neck of the vesicle just before the point of scission (Merrifield et al., 2002; Perrais and Merrifield, 2005).

One of the key molecules recruiting dynamin to endocytic vesicles is amphiphysin, which binds preferentially to membrane with high curvature, such as occurs at the vesicle neck (Peter et al., 2004). We find that introduction of an amphiphysin truncation mutant that cannot bind dynamin or synaptojanin 1 leads to a distinctive phenotype, the selective inhibition of fast events (Fig. 9). This might be explained if amphiphysin normally acts to accelerate closure of the vesicle mouth through an action requiring the SH3 domain. This action is unlikely to be simply the recruitment of dynamin because vesicle opening was not obviously affected by introduction of amphiphysin-SH3 at concentrations sufficient to block membrane scission (Fig. 8 B). The role of the actin cytoskeleton may be worth considering. Proteins containing BAR domains are often involved in membrane remodelling through the cytoskeleton (Itoh and De Camilli, 2006; Yamada et al., 2007), and Felmy (2007) has recently demonstrated that the time course of cargo release from dense-core vesicles is modulated by the actin cytoskeleton in PC12 cells. Exocytosis of granules in sea urchin eggs (Yu and Bement, 2007) and pancreatic acinar cells (Nemoto et al., 2004) is followed by the assembly of actin coats that have been suggested to stabilize the membrane invagination or promote their retrieval from the cell surface.

The molecular events involved in regulating the fusion and fission of secretory vesicles have been studied in detail; using IRM we now have a real-time assay that will allow us to study the intervening events that control opening and closing of the connection that mediates regulated secretion.

## Materials and methods

### Cell preparation and solutions

Bovine adrenal chromaffin cells were prepared as previously described (Llobet et al., 2003). Cells were plated onto poly-L-lysine (Sigma-Aldrich)-coated coverslips and used 1–3 d after preparation, when they were perfused with Ringer's solution containing 140 mM NaCl, 2.5 mM KCl, 1 mM  $\text{MgCl}_2$ , 10 mM Hepes, 10 mM glucose, and 2.5 mM  $\text{CaCl}_2$ , pH 7.4, 300 mOsm/kg. Intracellular patch solution contained 120 mM Cs-methanesulfonate, 10 mM TEA-Cl, 5 mM  $\text{MgCl}_2$ , 20 mM Hepes, 3 mM  $\text{Na}_2\text{ATP}$ , and 1 mM NaGTP, pH 7.2, 290 mOsm/kg. Variable amounts of calcium buffer were added, either 0.1–5.0 mM EGTA or 0.4 mM BAPTA. For uncaging experiments, calcium buffer was replaced by a 70% mixture of  $\text{CaCl}_2$  and NP-EGTA (provided by G. Ellis-Davies, Drexel University, Philadelphia, PA) and 0.3 mM Fura-2 or Fura-FF (Invitrogen). For measurements of the submembranous calcium concentration by TIRF microscopy, the calcium buffer in the intracellular solution was 0.2 mM Fluo-5N ( $K_d = 90 \mu\text{M}$ ; Invitrogen). Experiments were performed after 2 min of dialysis with the calcium-sensitive dye. The intracellular calcium concentration was calculated as  $[\text{Ca}^{2+}] = K_d (F - F_0)/(F_0)$  (Helmchen, 2000), where  $F_0$  is the resting level of fluorescence. All experiments were conducted at room temperature.

To test whether IRM events coincided with release of vesicle contents (Fig. 2), chromaffin cells were stimulated by local application of a depolarizing solution containing 50 mM KCl. To visualize dense-core vesicles, cells were transfected with ANP-GFP (provided by E.S. Levitan, University of Pittsburgh, Pittsburgh, PA; Johns et al., 2001). Transfection was performed using an Electro Square Porator (BTX). Another approach to loading vesicles was to incubate cells for 3 min in a solution containing 3  $\mu\text{M}$  of acridine orange, after which they were washed for 5–10 min.

### Combined capacitance and IRM measurements

IRM imaging was performed using an inverted microscope (Axiovert 200; Carl Zeiss, Inc.) as described previously (Llobet et al., 2003). All images and videos are displayed as difference images in which the background was subtracted using an average of 25 images obtained before stimulation. Difference images therefore display areas where the IRM image altered in response to stimulation (Llobet et al., 2003). Cells were voltage clamped in the whole-cell configuration using an amplifier (Axopatch 200A; MDS Analytical Technologies) and data were acquired with a computer (G4; Macintosh) equipped with an ITC-16 interface (InstruTECH) controlled by the pulse control extension (Horrigan and Bookman, 1994) of Igor Pro software (Wavemetrics). A detailed description on the methodology used to perform capacitance measurements has been described previously (Neves and Lagnado, 1999).

Exocytosis was triggered with either a 500-ms depolarization from  $-80$  to  $+10$  mV or with a train of  $24 \times 105$ -ms depolarizations from  $-80$  to  $+10$  mV delivered at 5 Hz. Image acquisition was performed using a charge-coupled device (CCD) camera (either QI-Cam [Q-Imaging] or PXL [Photometrics]) operated using IPLab software (BD Biosciences) at a rate of 55 Hz. Acquisition of images was triggered by a TTL pulse delivered by the ITC-16 at the beginning of the electrophysiological recording. To combine IRM experiments with  $\text{Ca}^{2+}$  uncaging, a bifurcated fiber bundle was used in combination with a 100-W Hg lamp equipped with two condensers. One half of the bundle allowed slow photolysis of NP-EGTA and simultaneous measurement of free  $[\text{Ca}^{2+}]$  by interleaving an exposure to 340 and 380 nm of light every 0.5 s. The other half of the bundle carried blue light for IRM imaging (485DF22 filter; Omega Optical Inc.). The filter block in the microscope was equipped with a dichroic mirror (500 DRLP; Omega Optical Inc.) that transmitted the green fluorescence emission of Fura-2 efficiently while only transmitting  $\sim 50\%$  of the blue light generating the IRM image. A dichroic mirror (505 DRLP; Omega Optical Inc.) located in a special mounting (Cairn Research Ltd) reflected the blue IRM image to a CCD camera while transmitting the green Fura-2 emission to a photomultiplier tube.

### Quantification of IRM signals

The method by which we quantified the dynamics of granule dilation and constriction was to simply measure changes in the total amount of reflected light because this signal was reproducible and obvious. We did not attempt to measure the actual diameter of the opening because the point-spread function of the microscope did not allow objects 200 nm in diameter to be discriminated from objects 2 nm in diameter (the suggested diameter of a putative fusion pore; Lindau and Alvarez de Toledo, 2003). The amplitude and spatial properties of the IRM signal are also expected to carry information about features that one might want to measure, such as the size of the opening to the granule and the size and shape of the

granule itself, but the quantitative analysis of IRM signals is too complex to obtain reliable estimates of these (Gingell and Todd, 1979). The time course of fusion events was assessed by an iterative process. First, a square ROI (252 nm across) was placed over the area where a spot appeared in the video of the IRM signal, as assessed by eye. The time course of the change in intensity over this region was plotted to identify the frame in which the signal was at a maximum. This single frame was then used to recenter the ROI over the pixel in which the signal was highest and the time course was measured again. To average events or compare their kinetics, time 0 was defined as the frame in which the signal peaked. Footprints selected for analysis typically contained four to six fusion events synchronous with the stimulus.

### Does the granule matrix contribute to the IRM signal?

The interior of a secretory granule contains a proteinaceous matrix that is osmophilic and appears dense in electron micrographs (Fig. 1 A). Might this matrix contribute to the signal observed at sites of granule fusion? In principle, the site of granule fusion might also appear brighter if the contents of the omega shape had a refractive index comparable to the cell membrane, increasing the amount of reflected light (Gingell and Todd, 1979). In practice, the optical density of the granule core is probably closer to that of water (1.3) than a membrane bilayer ( $\sim 1.5$ ). A concentrated solution of proteins has a refractive index of  $\sim 1.4$  whereas dried protein has a refractive index of 1.58 (Barer and Joseph, 1954). Thus, although the fundamental process giving rise to a bright spot in the footprint is an omega-shaped deflection of the surface membrane, we cannot rule out the possibility that the proteinaceous core of the granule alters the amount of reflected light and, therefore, the contrast of the image. But the gradual brightening of a spot on granule fusion is very unlikely to reflect dissolution of the core because the speed with which a spot brightens depends on the cytoplasmic calcium concentration triggering fusion (Figs. 4–6).

### Combined TIRF microscopy and IRM imaging

IRM imaging of vesicle fusion was combined with TIRF microscopy to monitor submembranous calcium signals (Fig. 3) in a microscope (Axiovert 200; Carl Zeiss, Inc.), as described previously (Llobet et al., 2003; Beaumont et al., 2005). An argon laser (488 nm) provided the beam for TIRF microscopy through a 60 $\times$  objective (1.45 NA; Olympus). The light for IRM originated from a Xenon lamp (100W; Newport-Oriel) and was transmitted through a filter (510WB40; Omega Optical Inc.) before passing through a combining cube (Newport-Oriel). The filter block contained a dichroic (505 DRLP), which reflected  $>95\%$  at 488 nm and  $\sim 35\%$  at 510 nm, while transmitting  $>80\%$  at wavelengths  $>515$  nm. About 35% of reflection was sufficient for IRM if the Xenon lamp was at maximum power. When only TIRF microscopy was used, emitted light was filtered through a filter (HQ510LP; Chroma Technology Corp.) and a 488-nm notch filter (Coherent). When TIRF microscopy was combined with IRM, emitted light was filtered through a filter (545AF75; Omega Optical Inc.). Images were magnified 2.2 $\times$  before being acquired by a CCD camera (Pentamax; Princeton Instruments) and acquisition software (Winview32; Roper Scientific). Image acquisition was synchronized with the electrophysiological recording using a pulse generator (Master-8; AMPI). The membrane current and camera exposure signal time were digitized (20 kHz) and filtered (5 kHz) by a Digidata interface (1322A; MDS Analytical Technologies).

IRM imaging of vesicle fusion was also combined with TIRF microscopy to monitor loss of vesicle contents (Fig. 2). In this case, images were acquired sequentially using a microscope (IX-71; Olympus) equipped with a modified TIRF illumination system (IX2-RFAEVA-2) using a 60 $\times$  objective. A 99% reflective mirror was placed in the light path for TIRF illumination, allowing 1% of the light from the epi-illumination light source to be transmitted for IRM. The IRM and TIRF light sources were controlled independently using shutters (Uniblitz; Vincent Associates) and synchronized with image acquisition using a pulse generator. Images were acquired at 3 Hz using a camera (C-9100; Hamamatsu Photonics) controlled by Okawo software (Hamamatsu Photonics). Image analysis was performed using ImageJ.

### Online supplemental material

Four videos illustrating fusions visualized under IRM are shown in the online supplemental material. Video 1 is a typical IRM experiment where multiple synchronous and a single asynchronous event are observed. Video 2 shows the mean temporal profile of asynchronous events. Video 3 shows the mean time course of synchronous events. Video 4 shows fusion events triggered by slow uncaging of NP-EGTA. Online supplemental material is available at <http://www.jcb.org/cgi/content/full/jcb.200807034/DC1>.

The authors thank H. McMahon, W. Jockusch, and J. Gallop for preparing amphiphysin-SH3 and amphiphysin-ΔSH3.

A. Llobet is a researcher of the Servicio Nacional de Salud (Instituto de Salud Carlos III) sponsored by grant PI05-1050.

Submitted: 7 July 2008

Accepted: 4 August 2008

## References

- Albillos, A., G. Dernick, H. Horstmann, W. Almers, G. Alvarez de Toledo, and M. Lindau. 1997. The exocytotic event in chromaffin cells revealed by patch amperometry. *Nature*. 389:509–512.
- Ales, E., L. Tabares, J.M. Poyato, V. Valero, M. Lindau, and G. Alvarez de Toledo. 1999. High calcium concentrations shift the mode of exocytosis to the kiss-and-run mechanism. *Nat. Cell Biol.* 1:40–44.
- Artalejo, C.R., A. Elhamdani, and H.C. Palfrey. 2002. Sustained stimulation shifts the mechanism of endocytosis from dynamin-1-dependent rapid endocytosis to clathrin- and dynamin-2-mediated slow endocytosis in chromaffin cells. *Proc. Natl. Acad. Sci. USA*. 99:6358–6363.
- Barer, R., and S. Joseph. 1954. Refractometry of living cells. *Q. J. Microsc. Sci.* 95:399–423.
- Barg, S., C.S. Olofsson, J. Schriever-Abeln, A. Wendt, S. Gebre-Medhin, E. Renstrom, and P. Rorsman. 2002. Delay between fusion pore opening and peptide release from large dense-core vesicles in neuroendocrine cells. *Neuron*. 33:287–299.
- Beaumont, V., A. Llobet, and L. Lagnado. 2005. Expansion of calcium microdomains regulates fast exocytosis at a ribbon synapse. *Proc. Natl. Acad. Sci. USA*. 102:10700–10705.
- Becherer, U., M. Pasche, S. Nofal, D. Hof, U. Matti, and J. Rettig. 2007. Quantifying exocytosis by combination of membrane capacitance measurements and total internal reflection fluorescence microscopy in chromaffin cells. *PLoS ONE*. 2:e505.
- Benedeczy, I. 1983. The functional morphology of chromaffin cells. *Acta Biol. Hung.* 34:137–154.
- Bhalla, A., W.C. Tucker, and E.R. Chapman. 2005. Synaptotagmin isoforms couple distinct ranges of  $\text{Ca}^{2+}$ ,  $\text{Ba}^{2+}$  and  $\text{Sr}^{2+}$  concentration to SNARE-mediated membrane fusion. *Mol. Biol. Cell*. 16:4755–4764.
- Chow, R.H., L. von Ruden, and E. Neher. 1992. Delay in vesicle fusion revealed by electrochemical monitoring of single secretory events in adrenal chromaffin cells. *Nature*. 356:60–63.
- Elhamdani, A., F. Azizi, and C.R. Artalejo. 2006a. Double patch clamp reveals that transient fusion (kiss-and-run) is a major mechanism of secretion in calf adrenal chromaffin cells: high calcium shifts the mechanism from kiss-and-run to complete fusion. *J. Neurosci.* 26:3030–3036.
- Elhamdani, A., F. Azizi, E. Solomaha, H.C. Palfrey, and C.R. Artalejo. 2006b. Two mechanistically distinct forms of endocytosis in adrenal chromaffin cells: differential effects of SH3 domains and amphiphysin antagonism. *FEBS Lett.* 580:3263–3269.
- Ellis-Davies, G.C., and J.H. Kaplan. 1994. Nitrophenyl-EGTA, a photolabile chelator that selectively binds  $\text{Ca}^{2+}$  with high affinity and releases it rapidly upon photolysis. *Proc. Natl. Acad. Sci. USA*. 91:187–191.
- Felmy, F. 2007. Modulation of cargo release from dense core granules by size and actin network. *Traffic*. 8:983–997.
- Fulop, T., and C. Smith. 2006. Physiological stimulation regulates the exocytic mode through calcium activation of protein kinase C in mouse chromaffin cells. *Biochem. J.* 399:111–119.
- Fulop, T., S. Radabaugh, and C. Smith. 2005. Activity-dependent differential transmitter release in mouse adrenal chromaffin cells. *J. Neurosci.* 25:7324–7332.
- Gad, H., N. Ringstad, P. Low, O. Kjaerulf, J. Gustafsson, M. Wenk, G. Di Paolo, Y. Nemoto, J. Crun, M.H. Ellisman, et al. 2000. Fission and uncoating of synaptic clathrin-coated vesicles are perturbed by disruption of interactions with the SH3 domain of endophilin. *Neuron*. 27:301–312.
- Gingell, D., and I. Todd. 1979. Interference reflection microscopy. A quantitative theory for image interpretation and its application to cell-substratum separation measurement. *Biophys. J.* 26:507–526.
- Gong, L.W., G.A. de Toledo, and M. Lindau. 2007. Exocytotic catecholamine release is not associated with cation flux through channels in the vesicle membrane but  $\text{Na}^{+}$  influx through the fusion pore. *Nat. Cell Biol.* 9:915–922.
- Grynszpan-Winograd, O. 1971. Morphological aspects of exocytosis in the adrenal medulla. *Philos. Trans. R. Soc. Lond. B Biol. Sci.* 261:291–292.
- Helmchen, F. 2000. Calibration of fluorescent calcium indicators. In *Imaging Neurons: a Laboratory Manual*. R. Yuste, E. Lanni, and A. Konnerth, editors. Cold Spring Harbor Laboratory Press, Cold Spring Harbor, NY. 32.1–32.9.
- Henkel, A.W., and W. Almers. 1996. Fast steps in exocytosis and endocytosis studied by capacitance measurements in endocrine cells. *Curr. Opin. Neurobiol.* 6:350–357.
- Holroyd, P., T. Lang, D. Wenzel, P. De Camilli, and R. Jahn. 2002. Imaging direct, dynamin-dependent recapture of fusing secretory granules on plasma membrane lawns from PC12 cells. *Proc. Natl. Acad. Sci. USA*. 99:16806–16811.
- Horrigan, F.T., and R.J. Bookman. 1994. Releasable pools and the kinetics of exocytosis in adrenal chromaffin cells. *Neuron*. 13:1119–1129.
- Hurley, J.H., and B. Wendland. 2002. Endocytosis: driving membranes around the bend. *Cell*. 111:143–146.
- Itoh, T., and P. De Camilli. 2006. BAR, F-BAR (EFC) and ENTH/ANTH domains in the regulation of membrane-cytosol interfaces and membrane curvature. *Biochim. Biophys. Acta*. 1761:897–912.
- Johns, L.M., E.S. Levitan, E.A. Shelden, R.W. Holz, and D. Axelrod. 2001. Restriction of secretory granule motion near the plasma membrane of chromaffin cells. *J. Cell Biol.* 153:177–190.
- Lee, M.C., and R. Schekman. 2004. Cell biology. BAR domains go on a bender. *Science*. 303:479–480.
- Lindau, M., and G. Alvarez de Toledo. 2003. The fusion pore. *Biochim. Biophys. Acta*. 1641:167–173.
- Llobet, A., V. Beaumont, and L. Lagnado. 2003. Real-time measurement of exocytosis and endocytosis using interference of light. *Neuron*. 40:1075–1086.
- McMahon, H.T., and J.L. Gallop. 2005. Membrane curvature and mechanisms of dynamic cell membrane remodeling. *Nature*. 438:590–596.
- Merrifield, C.J., M.E. Feldman, L. Wan, and W. Almers. 2002. Imaging actin and dynamin recruitment during invagination of single clathrin-coated pits. *Nat. Cell Biol.* 4:691–698.
- Neher, E., and A. Marty. 1982. Discrete changes of cell membrane capacitance observed under conditions of enhanced secretion in bovine adrenal chromaffin cells. *Proc. Natl. Acad. Sci. USA*. 79:6712–6716.
- Nemoto, T., T. Kojima, A. Oshima, H. Bito, and H. Kasai. 2004. Stabilization of exocytosis by dynamic F-actin coating of zymogen granules in pancreatic acini. *J. Biol. Chem.* 279:37544–37550.
- Neves, G., and L. Lagnado. 1999. The kinetics of exocytosis and endocytosis in the synaptic terminal of goldfish retinal bipolar cells. *J. Physiol.* 515:181–202.
- Patzak, A., and H. Winkler. 1986. Exocytotic exposure and recycling of membrane antigens of chromaffin granules: ultrastructural evaluation after immunolabeling. *J. Cell Biol.* 102:510–515.
- Perrais, D., and C.J. Merrifield. 2005. Dynamics of endocytic vesicle creation. *Dev. Cell*. 9:581–592.
- Perrais, D., I. Kleppe, J. Taraska, and W. Almers. 2004. Recapture after exocytosis causes differential retention of protein in granules of bovine chromaffin cells. *J. Physiol.* 560:413–428.
- Peter, B.J., H.M. Kent, I.G. Mills, Y. Vallis, P.J. Butler, P.R. Evans, and H.T. McMahon. 2004. BAR domains as sensors of membrane curvature: the amphiphysin BAR structure. *Science*. 303:495–499.
- Praefcke, G.J., and H.T. McMahon. 2004. The dynamin superfamily: universal membrane tubulation and fission molecules? *Nat. Rev. Mol. Cell Biol.* 5:133–147.
- Rettig, J., and E. Neher. 2002. Emerging roles of presynaptic proteins in  $\text{Ca}^{++}$ -triggered exocytosis. *Science*. 298:781–785.
- Schmidt, W., A. Patzak, G. Lingg, H. Winkler, and H. Plattner. 1983. Membrane events in adrenal chromaffin cells during exocytosis: a freeze-etching analysis after rapid cryofixation. *Eur. J. Cell Biol.* 32:31–37.
- Shin, O.H., J.S. Rhee, J. Tang, S. Sugita, C. Rosenmund, and T.C. Sudhoff. 2003.  $\text{Sr}^{2+}$  binding to the  $\text{Ca}^{2+}$  binding site of synaptotagmin 1 C2B domain triggers fast exocytosis without stimulating SNARE interactions. *Neuron*. 37:99–108.
- Smith, C., and E. Neher. 1997. Multiple forms of endocytosis in bovine adrenal chromaffin cells. *J. Cell Biol.* 139:885–894.
- Steyer, J.A., H. Horstmann, and W. Almers. 1997. Transport, docking and exocytosis of single secretory granules in live chromaffin cells. *Nature*. 388:474–478.
- Sudhof, T.C. 2002. Synaptotagmins: why so many? *J. Biol. Chem.* 277:7629–7632.
- Takei, K., P.S. McPherson, S.L. Schmid, and P. De Camilli. 1995. Tubular membrane invaginations coated by dynamin rings are induced by GTP-γS in nerve terminals. *Nature*. 374:186–190.
- Takei, K., V.I. Slepnev, V. Haucke, and P. De Camilli. 1999. Functional partnership between amphiphysin and dynamin in clathrin-mediated endocytosis. *Nat. Cell Biol.* 1:33–39.



- Taraska, J.W., and W. Almers. 2004. Bilayers merge even when exocytosis is transient. *Proc. Natl. Acad. Sci. USA*. 101:8780–8785.
- Taraska, J.W., D. Perrais, M. Ohara-Imaizumi, S. Nagamatsu, and W. Almers. 2003. Secretory granules are recaptured largely intact after stimulated exocytosis in cultured endocrine cells. *Proc. Natl. Acad. Sci. USA*. 100:2070–2075.
- Tsuboi, T., and G.A. Rutter. 2003. Multiple forms of “kiss-and-run” exocytosis revealed by evanescent wave microscopy. *Curr. Biol.* 13:563–567.
- Tsuboi, T., H.T. McMahon, and G.A. Rutter. 2004. Mechanisms of dense core vesicle recapture following “kiss and run” (“cavcapture”) exocytosis in insulin-secreting cells. *J. Biol. Chem.* 279:47115–47124.
- Verschueren, H. 1985. Interference reflection microscopy in cell biology: methodology and applications. *J. Cell Sci.* 75:279–301.
- Wang, C.T., R. Grishanin, C.A. Earles, P.Y. Chang, T.F. Martin, E.R. Chapman, and M.B. Jackson. 2001. Synaptotagmin modulation of fusion pore kinetics in regulated exocytosis of dense-core vesicles. *Science*. 294:1111–1115.
- Wang, C.T., J.C. Lu, J. Bai, P.Y. Chang, T.F. Martin, E.R. Chapman, and M.B. Jackson. 2003. Different domains of synaptotagmin control the choice between kiss-and-run and full fusion. *Nature*. 424:943–947.
- Weber, I. 2003. Reflection interference contrast microscopy. *Methods Enzymol.* 361:34–47.
- Wigge, P., K. Kohler, Y. Vallis, C.A. Doyle, D. Owen, S.P. Hunt, and H.T. McMahon. 1997. Amphiphysin heterodimers: potential role in clathrin-mediated endocytosis. *Mol. Biol. Cell*. 8:2003–2015.
- Yamada, H., E. Ohashi, T. Abe, N. Kusumi, S.A. Li, Y. Yoshida, M. Watanabe, K. Tomizawa, Y. Kashiwakura, H. Kumon, et al. 2007. Amphiphysin 1 is important for actin polymerization during phagocytosis. *Mol. Biol. Cell*. 18:4669–4680.
- Yoshida, Y., M. Kinuta, T. Abe, S. Liang, K. Araki, O. Cremona, G. Di Paolo, Y. Moriyama, T. Yasuda, P. De Camilli, and K. Takei. 2004. The stimulatory action of amphiphysin on dynamin function is dependent on lipid bilayer curvature. *EMBO J.* 23:3483–3491.
- Yu, H.Y., and W.M. Bement. 2007. Control of local actin assembly by membrane fusion-dependent compartment mixing. *Nat. Cell Biol.* 9:149–159.